npj | Quantum Materials

www.nature.com/npjquantmats

ARTICLE OPEN

Check for updates

Experimental evidence for Zeeman spin–orbit coupling in layered antiferromagnetic conductors

R. Ramazashvili[1]✉, P. D. Grigoriev[2,3,4], T. Helm[5,6,7]✉, F. Kollmannsberger[5,6], M. Kunz[5,6,11], W. Biberacher[5], E. Kampert[7], H. Fujiwara[8], A. Erb[5,6], J. Wosnitza[7,9], R. Gross[5,6,10] and M. V. Kartsovnik[5]✉

Most of solid-state spin physics arising from spin–orbit coupling, from fundamental phenomena to industrial applications, relies on symmetry-protected degeneracies. So does the Zeeman spin–orbit coupling, expected to manifest itself in a wide range of antiferromagnetic conductors. Yet, experimental proof of this phenomenon has been lacking. Here we demonstrate that the Néel state of the layered organic superconductor κ-(BETS)$_2$FeBr$_4$ shows no spin modulation of the Shubnikov–de Haas oscillations, contrary to its paramagnetic state. This is unambiguous evidence for the spin degeneracy of Landau levels, a direct manifestation of the Zeeman spin–orbit coupling. Likewise, we show that spin modulation is absent in electron-doped Nd$_{1.85}$Ce$_{0.15}$CuO$_4$, which evidences the presence of Néel order in this cuprate superconductor even at optimal doping. Obtained on two very different materials, our results demonstrate the generic character of the Zeeman spin–orbit coupling.

npj Quantum Materials (2021)6:11 ; https://doi.org/10.1038/s41535-021-00309-6

INTRODUCTION

Spin–orbit coupling (SOC) in solids intertwines electron orbital motion with its spin, generating a variety of fundamental effects[1,2]. Commonly, SOC originates from the Pauli term $\mathcal{H}_{\mathcal{P}} = \frac{\hbar}{4m_e^2}\boldsymbol{\sigma}\cdot\mathbf{p}\times\nabla V(\mathbf{r})$ in the electron Hamiltonian[3,4], where $\hbar$ is the Planck constant, m_e the free-electron mass, $\mathbf{p}$ the electron momentum, $\boldsymbol{\sigma}$ its spin, and $V(\mathbf{r})$ its potential energy depending on the position. Remarkably, Néel order may give rise to SOC of an entirely different nature, via the Zeeman effect[5,6]:

$$\mathcal{H}_{\mathcal{Z}}^{so} = -\frac{\mu_B}{2}\left[g_{\parallel}(\mathbf{B}_{\parallel}\cdot\boldsymbol{\sigma}) + g_{\perp}(\mathbf{k})(\mathbf{B}_{\perp}\cdot\boldsymbol{\sigma})\right], \tag{1}$$

where μ_B is the Bohr magneton, $\mathbf{k} = \mathbf{p}/\hbar$ the electron wave vector, $\mathbf{B}$ the magnetic field, while $g_{\parallel}$ and $g_{\perp}$ define the g-tensor components with respect to the Néel axis. In a purely transverse field $\mathbf{B}_{\perp}$, a hidden symmetry of a Néel antiferromagnet protects double degeneracy of Bloch eigenstates at a special set of momenta in the Brillouin zone (BZ)[5,6]: at such momenta, $g_{\perp}$ must vanish. The scale of $g_{\perp}$ is set by $g_{\parallel}$, which renders $g_{\perp}(\mathbf{k})$ substantially momentum dependent, and turns $\mathcal{H}_{\mathcal{Z}}^{so}$ into a veritable SOC[5–8]. This coupling was predicted to produce unusual effects, such as spin degeneracy of Landau levels in a purely transverse field $\mathbf{B}_{\perp}$[9,10] and spin-flip transitions, induced by an AC *electric* rather than magnetic field[10]. Contrary to the textbook Pauli SOC, this mechanism does not require heavy elements. Being proportional to the applied magnetic field (and thus tunable!), it is bound only by the Néel temperature of the given material. In addition to its fundamental importance, this distinct SOC mechanism opens new possibilities for spin manipulation, much sought after in the current effort[11–13] to harness electron spin for future spintronic applications. While the Zeeman SOC mechanism may be relevant to a vast variety of antiferromagnetic (AF) conductors such as chromium, cuprates, iron pnictides, hexaborides, borocarbides, as well as organic and heavy fermion compounds[6], it has not received an experimental confirmation yet.

Here we present experimental evidence for the spin degeneracy of Landau levels in two very different layered conductors, using Shubnikov–de Haas (SdH) oscillations as a sensitive tool for quantifying the Zeeman effect[14]. First, the organic superconductor κ-(BETS)$_2$FeBr$_4$ (hereafter κ-BETS)[15] is employed for testing the theoretical predictions. The key features making this material a perfect model system for our purposes are (i) a simple quasi-two-dimensional (quasi-2D) Fermi surface and (ii) the possibility of tuning between the AF and paramagnetic (PM) metallic states, both showing SdH oscillations, by a moderate magnetic field[15,16]. We find that, contrary to what happens in the PM state, the angular dependence of the SdH oscillations in the AF state of this compound is *not* modulated by the Zeeman splitting. We show that such a behavior is a natural consequence of commensurate Néel order giving rise to the Zeeman SOC in the form of Eq. (1).

Having established the presence of the Zeeman SOC in an AF metal, we utilize this effect for probing the electronic state of Nd$_{2-x}$Ce$_x$CuO$_4$ (NCCO), a prototypical example of electron-doped high-T_c cuprate superconductors[17]. In these materials, superconductivity coexists with another symmetry-breaking phenomenon manifested in a Fermi-surface reconstruction as detected by angle-resolved photoemission spectroscopy (ARPES)[18–21] and SdH experiments[22–25]. The involvement of magnetism in this Fermi-surface reconstruction has been broadly debated[26–41]. Here we present detailed data on the SdH amplitude in optimally doped NCCO, tracing its variation over more than two orders of magnitude with changing the field orientation. The oscillation behavior is found to be very similar to that in κ-BETS. Given the crystal symmetry and the position of the relevant Fermi-surface pockets, this result is firm evidence for antiferromagnetism

[1]Laboratoire de Physique Théorique, Université de Toulouse, CNRS, UPS, Toulouse, France. [2]L. D. Landau Institute for Theoretical Physics, Chernogolovka, Russia. [3]National University of Science and Technology MISiS, Moscow, Russia. [4]P. N. Lebedev Physical Institute, Moscow, Russia. [5]Walther-Meißner-Institut, Bayerische Akademie der Wissenschaften, Garching, Germany. [6]Physik-Department, Technische Universität München, Garching, Germany. [7]Hochfeld-Magnetlabor Dresden (HLD-EMFL) and Würzburg-Dresden Cluster of Excellence ct.qmat, Helmholtz-Zentrum Dresden-Rossendorf, Dresden, Germany. [8]Department of Chemistry, Graduate School of Science, Osaka Prefecture University, Osaka, Japan. [9]Institut für Festkörper- und Materialphysik, TU Dresden, Dresden, Germany. [10]Munich Center for Quantum Science and Technology (MCQST), Munich, Germany. [11]Present address: TNG Technology Consulting GmbH, Unterföhring, Germany. ✉email: revaz@irsamc.ups-tlse.fr; t.helm@hzdr.de; mark.kartsovnik@wmi.badw.de

in NCCO. Our finding not only settles the controversy in electron-doped cuprate superconductors but also clearly demonstrates the generality of the Zeeman SOC mechanism.

Before presenting the experimental results, we recapitulate the effect of Zeeman splitting on quantum oscillations. The superposition of the oscillations coming from the conduction subbands with opposite spins results in the well-known spin-reduction factor in the oscillation amplitude[14]: $R_s = \cos\left(\pi \frac{g}{2}\frac{m}{m_e}\right)$; here m_e and m are, respectively, the free-electron mass and the effective cyclotron mass of the relevant carriers. We restrict our consideration to the first-harmonic oscillations, which is fully sufficient for the description of our experimental results. In most three-dimensional (3D) metals, the dependence of R_s on the field orientation is governed by the anisotropy of the cyclotron mass. At some field orientations, R_s may vanish, and the oscillation amplitude becomes zero. This *spin-zero* effect carries information about the renormalization of the product gm relative to its free-electron value $2m_e$. For 3D systems, this effect is obviously not universal. For example, in the simplest case of a spherical Fermi surface, R_s possesses no angular dependence whatsoever, hence no spin zeros. By contrast, in quasi-2D metals with their vanishingly weak interlayer dispersion such as in layered organic and cuprate conductors, spin zeros are[42–47] a robust consequence of the monotonic increase of the cyclotron mass, $m \propto 1/\cos\theta$, with tilting the field by an angle θ away from the normal to the conducting layers.

In an AF metal, the g-factor may acquire a $\mathbf{k}$ dependence through the Zeeman SOC mechanism. It becomes particularly pronounced in the purely transverse geometry, i.e., for a magnetic field normal to the Néel axis. In this case, R_s contains the factor $\overline{g}_\perp$ averaged over the cyclotron orbit, see Supplementary Note I for details. As a result, the spin-reduction factor in a layered AF metal takes the form:

$$R_s = \cos\left[\frac{\pi}{\cos\theta}\frac{\overline{g}_\perp m_0}{2m_e}\right], \qquad (2)$$

where $m_0 \equiv m(\theta = 0°)$. Often, the Fermi surface is centered at a point $\mathbf{k}^*$, where the equality $g_\perp(\mathbf{k}^*) = 0$ is protected by symmetry[6] — as it is for κ-BETS (see Supplementary Note II). Such a $\mathbf{k}^*$ belongs to a line node $g_\perp(\mathbf{k}) = 0$ crossing the Fermi surface. Hence, $g_\perp(\mathbf{k})$ changes sign along the Fermi surface, and $\overline{g}_\perp$ in Eq. (2) vanishes by symmetry of $g_\perp(\mathbf{k})$. Consequently, the quantum-oscillation amplitude is predicted to have *no spin zeros*[9]. For pockets with Fermi wave vector k_F well below the inverse AF coherence length $1/\xi$, $g_\perp(\mathbf{k})$ can be described by the leading term of its expansion in $\mathbf{k}$. For such pockets, the present result was obtained in refs. [9,10,48]. According to our estimates in the Supplementary Note III, both in κ-BETS and in optimally doped NCCO ($x = 0.15$), the product $k_F\xi$ considerably exceeds unity. Yet, the quasi-classical consideration above shows that for $k_F\xi > 1$ the conclusion remains the same: $\overline{g}_\perp = 0$, see Supplementary Note IV for the explicit theory.

We emphasize that centering of the Fermi surface at a point $\mathbf{k}^*$ with $g_\perp(\mathbf{k}^*) = 0$ such as a high-symmetry point of the magnetic BZ boundary[6] — is crucial for a vanishing of $\overline{g}_\perp$. Otherwise, Zeeman SOC remains inert, as it does in AF $CeIn_3$, whose d Fermi surface is centered at the Γ point (see Supplementary Note V and refs. [49–51]), and in quasi-2D AF $EuMnBi_2$, with its quartet of Dirac cones centered away from the magnetic BZ boundary[52,53]. With this, we turn to the experiment.

RESULTS

AF organic superconductor κ-$(BETS)_2FeBr_4$

This is a quasi-2D metal with conducting layers of BETS donor molecules, sandwiched between insulating $FeBr_4^-$-anion layers[15]. The material has a centrosymmetric orthorhombic crystal structure (space group *Pnma*), with the *ac* plane along the layers. The Fermi surface consists of a weakly warped cylinder and two open sheets, separated from the cylinder by a small gap Δ_0 at the BZ boundary, as shown in Fig. 1[15,16,54].

The magnetic properties of the compound are mainly governed by five localized 3d-electron spins per Fe^{3+} ion in the insulating layers. Below $T_N \approx 2.5$ K, these $S = 5/2$ spins are ordered antiferromagnetically, with the unit cell doubling along the c axis and the staggered magnetization pointing along the a axis[15,55]. Above a critical magnetic field $B_c \sim 2$–5 T, dependent on the field orientation, antiferromagnetism gives way to a saturated PM state[56].

The SdH oscillations in the high-field PM state and in the Néel state are markedly different (see Fig. 1b). In the former, two dominant frequencies corresponding to a classical orbit α on the Fermi cylinder and to a large magnetic breakdown (MB) orbit β are found, in agreement with the predicted Fermi surface[16,54].

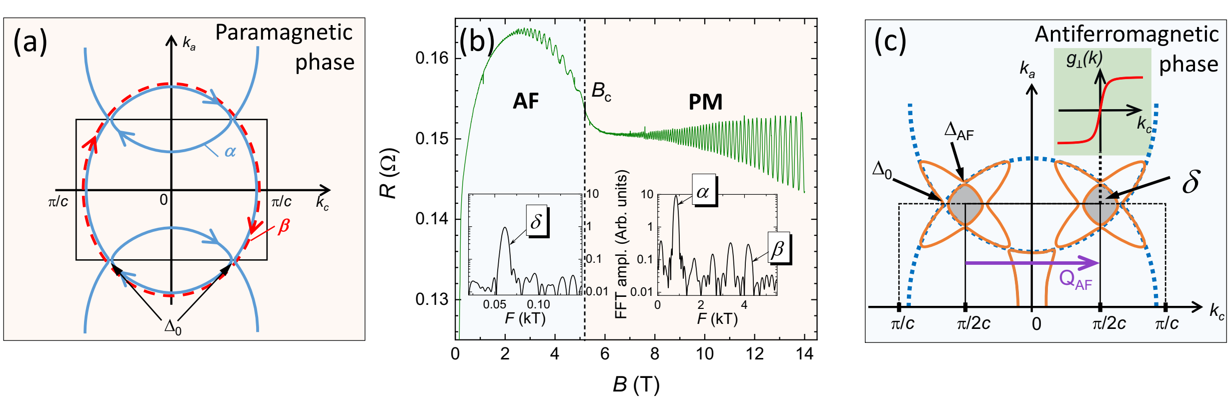

Fig. 1 2D Fermi surface of κ-BETS in the paramagnetic and antiferromagnetic phases. a Fermi surface of κ-BETS in the PM state[15,54] (blue lines). The blue arrows show the classical cyclotron orbits α and the red arrows the large MB orbit β, which involves tunneling through four MB gaps Δ_0 in a strong magnetic field. **b** Interlayer magnetoresistance of the κ-BETS sample, recorded at $T = 0.5$ K with field applied nearly perpendicularly to the layers ($\theta = 2°$). The vertical dashed line indicates the transition between the low-field AF and high-field PM states. The insets show the fast Fourier transforms (FFT) of the SdH oscillations for field windows [2–5] T and [12–14] T in the AF and PM state, respectively. **c** The BZ boundaries in the AF state with the wave vector $\mathbf{Q}_{AF} = (\pi/c, 0)$ and in the PM state are shown by solid-black and dashed-black lines, respectively. The dotted-blue and solid-orange lines show, respectively, the original and reconstructed Fermi surfaces[16]. The shaded area in the corner of the magnetic BZ, separated from the rest of the Fermi surface by gaps Δ_0 and Δ_{AF}, is the δ pocket responsible for the SdH oscillations in the AF state. The inset shows the function $g_\perp(\mathbf{k})$.

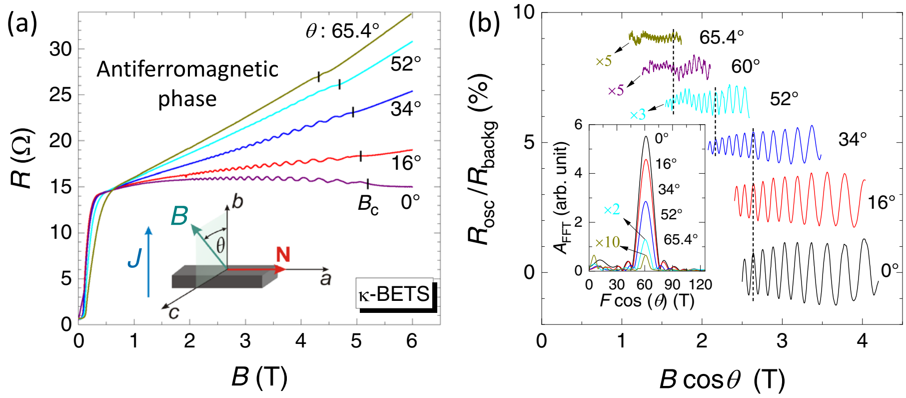

Fig. 2 SdH oscillations in the antiferromagnetic phase of κ-BETS. a Examples of the field-dependent interlayer resistance at different field orientations, at $T = 0.42$ K. The AF–PM transition field B_c is marked by vertical dashes. Inset: the orientation of the current **J** and magnetic field **B** relative to the crystal axes and the Néel axis **N**. **b** Oscillating component, normalized to the non-oscillating B-dependent resistance background, plotted as a function of the out-of-plane field component $B_\perp = B\cos\theta$. The curves corresponding to different tilt angles θ are vertically shifted for clarity. For $\theta \geq 52°$ the ratio R_{osc}/R_{backg} is multiplied by a constant factor, as indicated. The vertical dashed lines are drawn to emphasize the constant oscillation phase in these coordinates. Inset: FFT spectra of the SdH oscillations taken in the field window [3–4.2] T. The FFT amplitudes at $\theta = 52°$ and $65.4°$ are multiplied by a factor of 2 and 10, respectively.

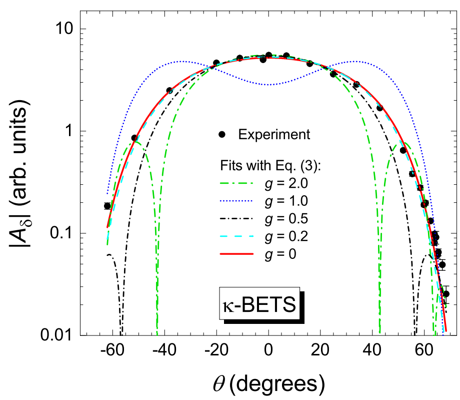

Fig. 3 Angular dependence of the SdH amplitude A_δ in the AF state of κ-BETS. The lines are fits using Eq. (3) with different values of the g-factor. The vertical error bars are determined by the signal-to-noise ratio of the corresponding FFT spectra.

The oscillation amplitude exhibits spin zeros as a function of the field strength and orientation, which is fairly well described by a field-dependent spin-reduction factor $R_s(\theta, B)$, with the g-factor $g = 2.0 \pm 0.2$ in the presence of an exchange field $B_J \approx -13$ T, imposed by PM Fe^{3+} ions on the conduction electrons[46,57]. In the Supplementary Note VI, we provide further details of the SdH oscillation studies on κ-BETS.

Below B_c, in the AF state, new, slow oscillations at the frequency $F_\delta \approx 62$ T emerge, indicating a Fermi-surface reconstruction[16]. The latter is associated with the folding of the original Fermi surface into the magnetic BZ, and F_δ is attributed to the new orbit δ, see Fig. 1c. This orbit emerges due to the gap Δ_{AF} at the Fermi-surface points, separated by the Néel wave vector $(\pi/c, 0)$[58].

Figure 2 shows examples of the field-dependent interlayer resistance of κ-BETS, recorded at $T = 0.42$ K, at different tilt angles θ. The field was rotated in the plane normal to the Néel axis (crystallographic a axis). In excellent agreement with previous reports[16,59], slow oscillations with frequency $F_\delta = 61.2\,\mathrm{T}/\cos\theta$ are observed below B_c, see inset in Fig. 2b. Thanks to the high crystal quality, even in this low-field region the oscillations can be traced over a wide angular range $|\theta| \leq 70°$.

The angular dependence of the δ-oscillation amplitude A_δ is shown in Fig. 3. The amplitude was determined by fast Fourier transform (FFT) of the zero-mean oscillating magnetoresistance component normalized to the monotonic B-dependent background, in the field window between 3.0 and 4.2 T, so as to stay below $B_c(\theta)$ for all field orientations. The lines in Fig. 3 are fits using the Lifshitz–Kosevich formula for the SdH amplitude[14]:

$$A_\delta = A_0 \frac{m^2}{\sqrt{B}} R_{MB} \frac{\exp(-KmT_D/B)}{\sinh(KmT/B)} R_s(\theta) \;, \tag{3}$$

where A_0 is a field-independent prefactor, $B = 3.5$ T (the midpoint of the FFT window in $1/B$ scale), m the effective cyclotron mass ($m = 1.1m_e$ at $\theta = 0°$[16], growing as $1/\cos\theta$ with tilting the field as in other quasi-2D metals[60,61]), $K = 2\pi^2 k_B/\hbar e$, $T = 0.42$ K, T_D the Dingle temperature, and R_{MB} the MB factor. For κ-BETS, R_{MB} takes the form $R_{MB} = \left[1 - \exp\left(-\frac{B_0}{B\cos\theta}\right)\right]\left[1 - \exp\left(-\frac{B_{AF}}{B\cos\theta}\right)\right]$, with two characteristic MB fields B_0 and B_{AF} associated with the gaps Δ_0 and Δ_{AF}, respectively. The Zeeman splitting effect is encapsulated in the spin factor $R_s(\theta)$. In Eq. (1), the geometry of our experiment implies $\mathbf{B}_\parallel = 0$, thus in the Néel state $R_s(\theta)$ takes the form of Eq. (2).

Excluding $R_s(\theta)$, the other factors in Eq. (3) decrease monotonically with increasing θ. By contrast, $R_s(\theta)$ in Eq. (2), generally, has an oscillating angular dependence. For $\bar{g}_\perp = g = 2.0$ found in the PM state[46], Eq. (2) yields two spin zeros, at $\theta \approx 43°$ and $64°$. Contrary to this, we observe *no* spin zeros but rather a monotonic decrease of A_δ by over two orders of magnitude as the field is tilted away from $\theta = 0°$ to $\pm 70°$, i.e., in the entire angular range where we observe the oscillations. The different curves in Fig. 3 are our fits using Eq. (3) with A_0 and T_D as fit parameters and different values of the g-factor. We used the MB field values $B_0 = 20$ T and $B_{AF} = 5$ T. While the exact values of B_0 and B_{AF} are unknown, they have virtually no effect on the fit quality, as we demonstrate in Supplementary Note VII. The best fit is achieved with $g = 0$, i.e., with an angle-independent spin factor $R_s = 1$. The excellent agreement between the fit and the experimental data confirms the quasi-2D character of the electron conduction, with the $1/\cos\theta$ dependence of the cyclotron mass.

Comparison of the curves in Fig. 3 with the data rules out $\bar{g}_\perp > 0.2$. Given the experimental error bars, we cannot exclude a nonzero $\bar{g}_\perp \lesssim 0.2$, yet even such a small finite value would be in stark contrast with the textbook $g = 2.0$, found from the SdH oscillations in the high-field, PM state[46]. Below we argue that, in fact, $\bar{g}_\perp$ in the Néel state is *exactly* zero.

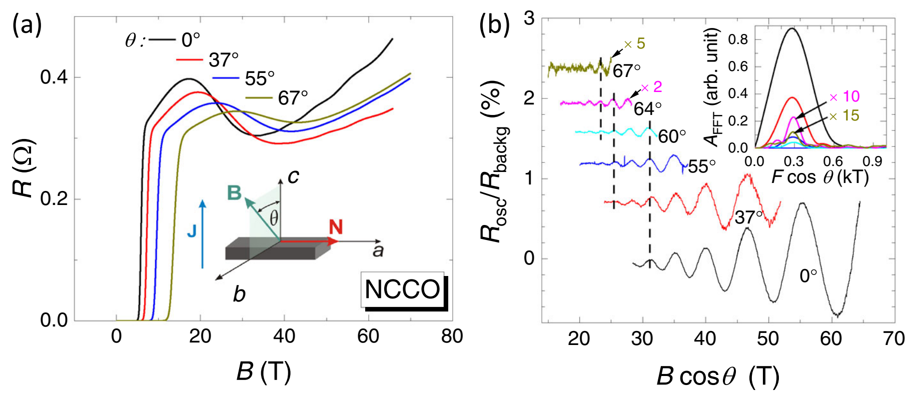

Fig. 4 Examples of magnetoresistance and angle-dependent SdH oscillations in optimally doped NCCO. a Examples of the B-dependent interlayer resistance at different field orientations, at $T = 2.5$ K. Inset: the orientation of the current **J** and magnetic field **B** relative to the crystal axes and the Néel axis **N**. **b** Oscillating component, normalized to the non-oscillating B-dependent resistance background, plotted as a function of the out-of-plane field component $B_\perp = B\cos\theta$. The curves corresponding to different tilt angles θ are vertically shifted for clarity. For $\theta = 64°$ and 67°, the ratio R_{osc}/R_{backg} is multiplied by a factor of 2 and 5, respectively. The vertical dashed lines are drawn to emphasize the constant oscillation phase in these coordinates; inset: FFT spectra of the SdH oscillations taken in the field window [45–64] T.

Optimally doped NCCO

This material has a body-centered tetragonal crystal structure (space group $I4/mmm$), where (001) conducting CuO_2 layers alternate with their insulating $(Nd,Ce)O_2$ counterparts[17]. Band-structure calculations[62,63] predict a hole-like cylindrical Fermi surface, centered at the corner of the BZ. However, ARPES[18–21,64] reveals a reconstruction of this Fermi surface by a $(\pi/a, \pi/a)$ order. Moreover, magnetic quantum oscillations[23–25] show that the Fermi surface remains reconstructed even in the overdoped regime, up to the critical doping x_c (≈ 0.175 for NCCO), where the superconductivity vanishes[65]. The origin of this reconstruction remains unclear: while the $(\pi/a, \pi/a)$ periodicity is compatible with the Néel order observed in strongly underdoped NCCO, coexistence of antiferromagnetism and superconductivity in electron-doped cuprates remains controversial. A number of neutron-scattering and muon-spin rotation studies[32–35] have detected short-range Néel fluctuations but no static order within the superconducting doping range. However, other neutron scattering[36,37] and magnetotransport[38–40] experiments have produced evidence of static or quasi-static AF order in superconducting samples at least up to optimal doping x_{opt}. Alternative mechanisms of the Fermi-surface reconstruction have been proposed, including a d-density wave[28], a charge-density wave[29], or coexistent topological and fluctuating short-range AF orders[30,31].

To shed light on the relevance of antiferromagnetism to the electronic ground state of superconducting NCCO, we have studied the field-orientation dependence of the SdH oscillations of the interlayer resistance in an optimally doped, $x_{opt} = 0.15$, NCCO crystal. The overall magnetoresistance behavior is illustrated in Fig. 4a. At low fields, the sample is superconducting. Immediately above the θ-dependent superconducting critical field, the magnetoresistance displays a non-monotonic feature, which has already been reported for optimally doped NCCO in a magnetic field normal to the layers[22,66]. This anomaly correlates with an anomaly in the Hall resistance and has been associated with MB through the energy gap, created by the $(\pi/a, \pi/a)$-superlattice potential[65]. With increasing θ, the anomaly shifts to higher fields, consistently with the expected increase of the breakdown gap with tilting the field.

SdH oscillations develop above about 30 T. Figure 4b shows examples of the oscillatory component of the magnetoresistance, normalized to the field-dependent non-oscillatory background resistance R_{backg}, determined by a low-order polynomial fit to the as-measured $R(B)$ dependence. In our conditions, $B \lesssim 65$ T,

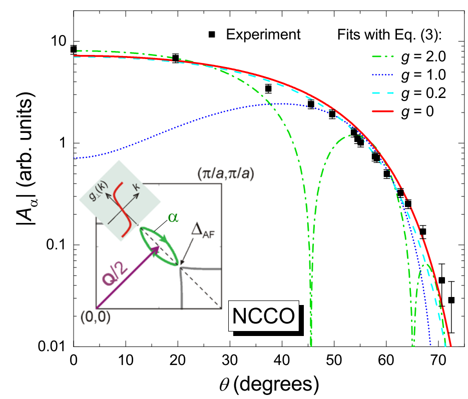

Fig. 5 Angular dependence of the SdH amplitude in optimally doped NCCO. The lines are fits using Eq. (3) with different g-factor values. Inset: The first quadrant of the BZ with the Fermi surface reconstructed by a superlattice potential with wave vector $\mathbf{Q} = (\pi/a, \pi/a)$. If this potential involves Néel order, the function $g_\perp(\mathbf{k})$ (red line in the inset) vanishes at the reduced BZ boundary (dashed line). The SdH oscillations are associated with the oval hole pocket α centered at $(\pi/2a, \pi/2a)$[22]. The error bars are defined as described in Supplementary Note VIII.

$T = 2.5$ K, the only discernible contribution to the oscillations comes from the hole-like pocket α of the reconstructed Fermi surface[22]. This pocket is centered at the reduced BZ boundary, as shown in the inset of Fig. 5. While MB creates large cyclotron orbits β with the area equal to that of the unreconstructed Fermi surface, even in fields of 60–65 T the fast β oscillations are more than two orders of magnitude weaker than the α oscillations[24,65].

The oscillatory signal is plotted in Fig. 4b as a function of the out-of-plane field component $B_\perp = B\cos\theta$. In these coordinates, the oscillation frequency remains constant, indicating that $F(\theta) = F(0°)/\cos\theta$ and thus confirming the quasi-2D character of the conduction. In the inset, we show the respective FFTs plotted against the $\cos\theta$-scaled frequency. They exhibit a peak at $F\cos\theta = 294$ T, in line with previous reports. The relatively large width of the FFT peaks is caused by the small number of oscillations in the field window [45–64] T. This restrictive choice is dictated by the requirement that the SdH oscillations be resolved over the whole field window at all tilt angles up to $\theta \approx 72°$. In Supplementary Note VIII, we provide an additional analysis of the amplitude at fixed field values, confirming the FFT results.

Furthermore, in Fig. 4b one can see that the phase of the oscillations is not inverted and stays constant in the studied angular range. This is fully in line with the absence of spin zeros, see Eq. (2).

The main panel of Fig. 5 presents the angular dependence of the oscillation amplitude (symbols), in a field rotated in the (*ac*) plane. The amplitude was determined by FFT of the data taken at $T = 2.5$ K in the field window $45\,\mathrm{T} \le B \le 64\,\mathrm{T}$. The lines in the figure are fits using Eq. (3), for different *g*-factors. The fits were performed using the MB factor $R_{MB} = [1 - \exp(-B_0/B)]$[24,65], the reported values for the MB field $B_0 = 12.5$ T, and the effective cyclotron mass $m(\theta = 0°) = 1.05 m_0$[65], while taking into account the $1/\cos\theta$ angular dependence of both B_0 and m. The prefactor A_0 and Dingle temperature T_D were used as fit parameters, yielding $T_D = (12.6 \pm 1)$ K, close to the value found in the earlier experiment[65]. Note that, contrary to the hole-doped cuprate $YBa_2Cu_3O_{7-x}$, where the analysis of earlier experiments[47,67] was complicated by the bilayer splitting of the Fermi cylinder[47], the single-layer structure of NCCO poses no such difficulty.

Similar to κ-BETS, the oscillation amplitude in NCCO decreases by a factor of about 300, with no sign of spin zeros as the field is tilted from $\theta = 0°$ to $72.5°$. Again, this behavior is incompatible with the textbook value $g = 2$, which would have produced two spin zeros in the interval $0° \le \theta \le 70°$, see the green dash-dotted line in Fig. 5. A reduction of the *g*-factor to 1.0 would shift the first spin zero to about 72°, near the edge of our range (blue dotted line in Fig. 5). However, this would simultaneously suppress the amplitude at small θ by a factor of ten, contrary to our observations. All in all, our data rule out a constant $g > 0.2$.

DISCUSSION

In both materials, our data impose on the effective *g*-factor an upper bound of 0.2. At first sight, one could simply view this as a suppression of the effective *g* to a small nonzero value. However, below we argue that, in fact, our findings imply $\overline{g}_\perp = 0$ and point to the importance of the Zeeman SOC in both materials. The quasi-2D character of electron transport is crucial for this conclusion: as mentioned above, in three dimensions, the mere absence of spin zeros imposes no bounds on the *g*-factor.

In κ-BETS, the interplay between the crystal symmetry and the periodicity of the Néel state[5,6,48] guarantees that $g_\perp(\mathbf{k})$ vanishes on the entire line $k_c = \pi/2c$ and is an odd function of $k_c - \pi/2c$, see the inset of Fig. 1c and Supplementary Figure 2 in Supplementary Note II. The δ orbit is centered on the line $k_c = \pi/2c$; hence $\overline{g}_\perp$ in Eq. (2) vanishes, implying the absence of spin zeros, in agreement with our data. At the same time, quantum oscillations in the PM phase clearly reveal the Zeeman splitting of Landau levels with $g = 2.0$[46]. Therefore, we conclude that $\overline{g}_\perp = 0$ is an intrinsic property of the Néel state.

In optimally doped NCCO, as already mentioned, the presence of a (quasi)static Néel order has been a subject of debate. However, if indeed present, such an order leads to $g_\perp(\mathbf{k}) = 0$ at the entire magnetic BZ boundary (see Supplementary Note II). For the hole pockets, producing the observed $F_\alpha \simeq 300$ T oscillations, $\overline{g}_\perp = 0$ by symmetry of $g_\perp(\mathbf{k})$ (see inset of Fig. 5 and Supplementary Fig. 3). Such an interpretation requires that the relevant AF fluctuations have frequencies below the cyclotron frequency in our experiment, $\nu_c \sim 10^{12}$ Hz at 50 T.

Finally, we address mechanisms — other than Zeeman SOC of Eq. (1) — that may also lead to the absence of spin zeros. While such mechanisms do exist, we will show that none of them is relevant to the materials of our interest.

When looking for alternative explanations to our experimental findings, let us recall that, generally, the effective *g*-factor may depend on the field orientation. This dependence may happen to compensate that of the quasi-2D cyclotron mass, $m_0/\cos\theta$, in the expression (2) for the spin-reduction factor R_s, and render the latter nearly isotropic, with no spin zeros. Obviously, such a compensation requires a strong Ising anisotropy $[g(\theta = 0°) \gg g(\theta = 90°)]$ — as found, for instance, in the heavy fermion compound URu_2Si_2, with the values $g_c = 2.65 \pm 0.05$ and $g_{ab} = 0.0 \pm 0.1$ for the field along and normal to the *c* axis, respectively[68,69]. However, this scenario is irrelevant to both materials of our interest: In κ-BETS, a nearly isotropic *g*-factor, close to the free-electron value 2.0, was revealed by a study of spin zeros in the PM state[46]. In NCCO, the conduction electron *g*-factor may acquire anisotropy via an exchange coupling to Nd^{3+} local moments. However, the low-temperature magnetic susceptibility of Nd^{3+} in the basal plane is some five times larger than along the *c* axis[70,71]. Therefore, the coupling to Nd^{3+} may only <u>increase</u> g_{ab} relative to g_c, and thereby only <u>enhance</u> the angular dependence of R_s rather than cancel it out. Thus we are led to rule out a *g*-factor anisotropy of crystal-field origin as a possible reason behind the absence of spin zeros in our experiments.

As follows from Eq. (2), another possible reason for the absence of spin zeros is a strong reduction of the ratio $gm/2m_e$. However, while *some* renormalization of this ratio in metals is commonplace, its dramatic suppression (let alone nullification) is, in fact, exceptional. First, a vanishing mass would contradict $m/m_e \ge 1$, experimentally found in both materials at hand. On the other hand, a Landau Fermi-liquid renormalization[14] $g \to g/(1 + G_0)$ would require a colossal Fermi-liquid parameter $G_0 \ge 10$, for which there is no evidence in NCCO, let alone κ-BETS with its already mentioned $g \approx 2$ in the PM state[46].

A sufficient difference of the quantum-oscillation amplitudes and/or cyclotron masses for spin-up and spin-down Fermi surfaces might also lead to the absence of spin zeros. Some heavy fermion compounds show strong spin polarization in magnetic field, concomitant with a substantial field-induced difference of the cyclotron masses of the two spin-split subbands[72,73]. As a result, for quantum oscillations in such materials, one spin amplitude considerably exceeds the other, and no spin zeros are expected. Note that this physics requires the presence of a very narrow conduction band, in addition to a broad one. In heavy fermion compounds, such a band arises from the *f* electrons but is absent in both materials of our interest.

Another extreme example is given by the single fully polarized band in a ferromagnetic metal, where only one spin orientation is present, and spin zeros are obviously absent. Yet, no sign of ferromagnetism or metamagnetism has been seen in either NCCO or κ-BETS. Moreover, in κ-BETS, the spin-zero effect has been observed in the PM state[46], indicating that the quantum-oscillation amplitudes of the two spin-split subbands are comparable. However, for NCCO one may inquire whether spin polarization could render interlayer tunneling amplitudes for spin-up and spin-down different enough to lose spin zeros, especially in view of an extra contribution of Nd^{3+} spins in the insulating layers to spin polarization. In Supplementary Note IX, we show that this is *not* the case.

Thus we are led to conclude that the absence of spin zeros in the AF κ-BETS and in optimally doped NCCO is indeed a manifestation of the Zeeman SOC. Our explanation relies only on the symmetry of the Néel state and the location of the carrier pockets, while being insensitive to the mechanism of the antiferromagnetism or to the orbital makeup of the relevant bands.

METHODS

Crystal preparation

Crystals of κ-$(BETS)_2FeBr_4$ were grown electrochemically and prepared for transport measurements as reported previously[46].

Optimally doped single crystals of $Nd_{1.85}Ce_{0.15}CuO_4$, grown by the traveling solvent floating zone method, were prepared for transport measurements as reported previously[22].

Magnetotransport measurements on κ-BETS

The interlayer ($I||b$) resistance was measured by the standard four-terminal a.c. technique using a low-frequency lock-in amplifier. Magnetoresistance measurements were performed in a superconducting magnet system at fields of up to 14 T. The samples were mounted on a holder allowing in situ rotation of the sample around an axis perpendicular to the external field direction. The orientation of the crystal was defined by a polar angle θ between the field and the crystallographic b axis (normal to the conducting layers).

Magnetotransport measurements on NCCO

Measurements of the interlayer ($I||c$) resistance were performed on a rotatable platform using a standard four-terminal a.c. technique at frequencies of 30–70 kHz in a 70 T pulse-magnet system, with a pulse duration of 150 ms, at the Dresden High Magnetic Field Laboratory. The raw data were collected by a fast digitizing oscilloscope and processed afterwards by a digital lock-in procedure[22]. The orientation of the crystal was defined by a polar angle θ between the field and the crystallographic c axis (normal to the conducting layers).

DATA AVAILABILITY

The authors declare that all essential data supporting the findings of this study are available within the paper and its supplementary information. The complete data set in ASCII format is available from the corresponding authors upon reasonable request.

Received: 3 September 2020; Accepted: 28 December 2020;
Published online: 05 February 2021

REFERENCES

1. Winkler, R. *Spin-orbit Coupling Effects in Two-dimensional Electron and Hole Systems, Springer Tracts in Modern Physics*, Vol. 191 (Springer, Berlin, 2003).
2. Dyakonov, M. I. (ed.) *Spin Physics in Semiconductors, Springer Series in Solid-State Sciences*, Vol. 157 (Springer, Berlin, 2017).
3. Berestetskii, V. B., Lifshitz, E. M. & Pitaevskii, L. P. *Quantum Electrodynamics (Course of Theoretical Physics)*, Vol. 4 (Pergamon Press, 1982).
4. Kittel, C. Quantum Theory of Solids, 2nd ed. (John Willey & Sons, New York, 1987).
5. Ramazashvili, R. Kramers degeneracy in a magnetic field and Zeeman spin-orbit coupling in antiferromagnetic conductors. *Phys. Rev. Lett.* **101**, 137202 (2008).
6. Ramazashvili, R. Kramers degeneracy in a magnetic field and Zeeman spin-orbit coupling in antiferromagnetic conductors. *Phys. Rev. B* **79**, 184432 (2009).
7. Brazovskii, S. A. & Luk'yanchuk, I. A. Symmetry of electron states in antiferromagnets. *Sov. Phys. JETP* **69**, 1180–1184 (1989).
8. Brazovskii, S. A., Luk'yanchuk, I. A. & Ramazashvili, R. R. Electron paramagnetism in antiferromagnets. *JETP Lett.* **49**, 644–646 (1989).
9. Kabanov, V. V. & Alexandrov, A. S. Magnetic quantum oscillations in doped antiferromagnetic insulators. *Phys. Rev. B.* **77**, 132403 (2008); erratum **81**, 099907 (2010).
10. Ramazashvili, R. Electric excitation of spin resonance in antiferromagnetic conductors. *Phys. Rev. B* **80**, 054405 (2009).
11. Rashba, E. I. & Sheka, V. I. in *Landau Level Spectroscopy* (eds Landwehr, G. & Rashba, E. I.) Ch. 4 (Elsevier, New York, 1991).
12. Shafiei, M., Nowack, K. C., Reichl, C., Wegscheider, W. & Vandersypen, L. M. K. Resolving spin-orbit- and hyperfine-mediated electric dipole spin resonance in a quantum dot. *Phys. Rev. Lett.* **110**, 107601 (2013).
13. van den Berg, J. W. G. et al. Fast spin-orbit qubit in an indium antimonide nanowire. *Phys. Rev. Let* **110**, 066806 (2013).
14. Shoenberg, D. *Magnetic Oscillations in Metals* (Cambridge University Press, Cambridge, 1984).
15. Fujiwara, H. et al. A novel antiferromagnetic organic superconductor κ-$(BETS)_2FeBr_4$ [where BETS = Bis(ethylenedithio)tetraselenafulvalene]. *J. Am. Chem. Soc.* **123**, 306–314 (2001).
16. Konoike, T. et al. Fermi surface reconstruction in the magnetic-field-induced superconductor κ-$(BETS)_2FeBr_4$. *Phys. Rev. B* **72**, 094517 (2005).
17. Armitage, N. P., Fournier, P. & Greene, R. L. Progress and perspectives on electron-doped cuprates. *Rev. Mod. Phys.* **82**, 2421–2487 (2010).
18. Santander-Syro, A. F. et al. Two-Fermi-surface superconducting state and a nodal d-wave energy gap of the electron-doped $Sm_{1.85}Ce_{0.15}CuO_{4-\delta}$ cuprate superconductor. *Phys. Rev. Lett.* **106**, 197002 (2011).
19. Song, D. et al. Electron number-based phase diagram of $Pr_{1-x}LaCe_xCuO_{4-\delta}$ and possible absence of disparity between electron- and hole-doped cuprate phase diagrams. *Phys. Rev. Lett.* **118**, 137001 (2017).
20. He, J.-F. et al. Fermi surface reconstruction in electron-doped cuprates without antiferromagnetic long-range order. *Proc. Natl Acad. Sci. USA.* **116**, 3449–3453 (2019).
21. Matsui, H. et al. Evolution of the pseudogap across the magnet-superconductor phase boundary of $Nd_{2-x}Ce_xCuO_4$. *Phys. Rev. B* **75**, 224514 (2007).
22. Helm, T. et al. Evolution of the Fermi surface of the electron-doped high-temperature superconductor $Nd_{2-x}Ce_xCuO_4$ revealed by Shubnikov–de Haas oscillations. *Phys. Rev. Lett.* **103**, 157002 (2009).
23. Helm, T. et al. Magnetic breakdown in the electron-doped cuprate superconductor $Nd_{2-x}Ce_xCuO_4$: the reconstructed Fermi surface survives in the strongly overdoped regime. *Phys. Rev. Lett.* **105**, 247002 (2010).
24. Kartsovnik, M. V. et al. Fermi surface of the electron-doped cuprate superconductor $Nd_{2-x}Ce_xCuO_4$ probed by high-field magnetotransport. *New J. Phys.* **13**, 015001 (2011).
25. Higgins, J. S. et al. Quantum oscillations from the reconstructed Fermi surface in electron-doped cuprate superconductors. *New J. Phys.* **20**, 043019 (2018).
26. Das, T., Markiewicz, R. S. & Bansil, A. Superconductivity and topological Fermi surface transitions in electron-doped cuprates near optimal doping. *J. Phys. Chem. Solids* **69**, 2963–2966 (2008).
27. Sachdev, S. Where is the quantum critical point in the cuprate superconductors? *Phys. Status Solidi B* **247**, 537–543 (2010).
28. Chakravarty, S., Laughlin, R. B., Morr, D. K. & Nayak, C. Hidden order in cuprates. *Phys. Rev. B* **63**, 094503 (2001).
29. da Silva Neto, E. H. et al. Charge ordering in the electron-doped superconductor $Nd_{2-x}Ce_xCuO_4$. *Science* **347**, 282–285 (2015).
30. Sachdev, S. Topological order, emergent gauge fields, and Fermi surface reconstruction. *Rep. Prog. Phys.* **82**, 014001 (2019).
31. Sachdev, S., Scammell, H. D., Scheurer, M. S. & Tarnopolsky, G. Gauge theory for the cuprates near optimal doping. *Phys. Rev. B* **99**, 054516 (2019).
32. Luke, G. M. et al. Magnetic order and electronic phase diagrams of electron-doped copper oxide materials. *Phys. Rev. B* **42**, 7981–7988 (1990).
33. Motoyama, E. M. et al. Spin correlations in the electron-doped high-transition-temperature superconductor $Nd_{2-x}Ce_xCuO_{4\pm\delta}$. *Nature* **445**, 186–189 (2007).
34. Mang, P. K. et al. Phase decomposition and chemical inhomogeneity in $Nd_{2-x}Ce_xCuO_{4\pm\delta}$. *Phys. Rev. B* **70**, 094507 (2004).
35. Saadaoui, H. et al. The phase diagram of electron-doped $La_{2-x}Ce_xCuO_{4-\delta}$. *Nat. Commun.* **6**, 6041 (2015).
36. Yamada, K. et al. Commensurate spin dynamics in the superconducting state of an electron-doped cuprate superconductor. *Phys. Rev. Lett.* **90**, 137004 (2003).
37. Kang, H. J. et al. Electronically competing phases and their magnetic field dependence in electron-doped nonsuperconducting and superconducting $Pr_{0.88}LaCe_{0.12}CuO_{4\pm\delta}$. *Phys. Rev. B* **71**, 214512 (2005).
38. Dagan, Y. et al. Origin of the anomalous low temperature upturn in the resistivity of the electron-doped cuprate superconductors. *Phys. Rev. Lett.* **94**, 057005 (2005).
39. Yu, W., Higgins, J. S., Bach, P. & Greene, R. L. Transport evidence of a magnetic quantum phase transition in electron-doped high-temperature superconductors. *Phys. Rev. B* **76**, 020503(R) (2007).
40. Dorantes, A. et al. Magnetotransport evidence for irreversible spin reorientation in the collinear antiferromagnetic state of underdoped $Nd_{2-x}Ce_xCuO_4$. *Phys. Rev. B* **97**, 054430 (2018).
41. Greene, R. L., Mandal, P. R., Poniatowski, N. R. & Sarkar, T. The strange metal state of the electron-doped cuprates. *Annu. Rev. Condens. Matter Phys.* **11**, 213–229 (2020).
42. Wosnitza, J. et al. De Haas-van Alphen studies of the organic superconductors α-$(ET)_2NH_4Hg(SCN)_4$ and κ-$(ET)_2Cu(NCS)_2$ with ET = bis(ethelenedithio)-tetrathiafulvalene. *Phys. Rev. B* **45**, 3018–3025 (1992).
43. Kovalev, A. E., Kartsovnik, M. V. & Kushch, N. D. Quantum and semi-classical magnetoresistance oscillations in a new organic metal $(BEDT\text{-}TTF)_2TlHg(SeCN)_4$. *Solid State Commun.* **87**, 705–708 (1993).
44. Meyer, F. A. et al. High-field de Haas-Van Alphen studies of κ-$(BEDT\text{-}TTF)_2Cu(NCS)_2$. *Europhys. Lett.* **32**, 681–686 (1995).
45. Uji, S. et al. Fermi surface and internal magnetic field of the organic conductors λ-$(BETS)_2Fe_xGa_{1-x}Cl4$. *Phys. Rev. B* **65**, 113101 (2002).
46. Kartsovnik, M. V. et al. Interplay between conducting and magnetic systems in the antiferromagnetic organic superconductor κ-$(BETS)_2FeBr_4$. *J. Supercond. Nov. Magn* **29**, 3075–3080 (2016).
47. Ramshaw, B. J. et al. Angle dependence of quantum oscillations in $YBa_2Cu_3O_{6.59}$ shows free-spin behaviour of quasiparticles. *Nat. Phys.* **7**, 234–238 (2011).
48. Ramazashvili, R. Quantum oscillations in antiferromagnetic conductors with small carrier pockets. *Phys. Rev. Lett.* **105**, 216404 (2010).

49. Settai, R. et al. De Haas - van Alphen studies of rare earth compounds. *J. Magn. Magn. Mater.* **140-144**, 1153–1154 (1995).
50. Ebihara, T., Harrison, N., Jaime, M., Uji, S. & Lashley, J. C. Emergent fluctuation hot spots on the Fermi surface of $CeIn_3$ in strong magnetic fields. *Phys. Rev. Lett.* **93**, 246401 (2004).
51. Gor'kov, L. P. & Grigoriev, P. D. Antiferromagnetism and hot spots in $CeIn_3$. *Phys. Rev. B* **73**, 060401(R) (2006).
52. Masuda, H. et al. Impact of antiferromagnetic order on Landau-level splitting of quasi-two-dimensional Dirac fermions in $EuMnBi_2$. *Phys. Rev. B* **98**, 161108(R) (2018).
53. Borisenko, S. et al. Time-reversal symmetry breaking type-II Weyl state in $YbMnBi_2$. *Nat. Commun.* **10**, 3424 (2019).
54. Uji, S. et al. Two-dimensional Fermi surface for the organic conductor κ-$(BETS)_2FeBr_4$. *Physica B* **298**, 557–561 (2001).
55. Mori, T. & Katsuhara, M. Estimation of πd -interactions in organic conductors including magnetic anions. *J. Phys. Soc. Jpn.* **71**, 826–844 (2002).
56. Konoike, T. et al. Magnetic-field-induced superconductivity in the anti-ferromagnetic organic superconductor κ-$(BETS)_2FeBr_4$. *Phys. Rev. B* **70**, 094514 (2004).
57. Cépas, O., McKenzie, R. H. & Merino, J. Magnetic-field-induced superconductivity in layered organic molecular crystals with localized magnetic moments. *Phys. Rev. B* **65**, 100502(R) (2002).
58. Peierls, R. E. *Quantum Theory of Solids* (Oxford University Press, Oxford, 2001).
59. Konoike, T. et al. Anomalous magnetic-field-hysteresis of quantum oscillations in κ-$(BETS)_2FeBr_4$. *J. Low Temp. Phys.* **142**, 531–534 (2006).
60. Wosnitza, J. *Fermi Surfaces of Low-Dimensional Organic Metals and Superconductors* (Springer Verlag, Berlin, 1996).
61. Kartsovnik, M. V. High magnetic fields: a tool for studying electronic properties of layered organic metals. *Chem. Rev.* **104**, 5737–5782 (2004).
62. Massidda, S., Hamada, N., Yu, J. & Freeman, A. J. Electronic structure of Nd-Ce-Cu-O, a Fermi liquid superconductor. *Physica C* **157**, 571–574 (1989).
63. Andersen, O. K., Liechtenstein, A. I., Jepsen, O. & Paulsen, F. LDA energy bands, low-energy Hamiltonians, t', t'', $t_{\perp}$(k), and $J_{\perp}$. *J. Phys. Chem. Solids* **56**, 1573–1591 (1995).
64. Armitage, N. P. et al. Doping dependence of an *n*-type cuprate superconductor investigated by angle-resolved photoemission spectroscopy. *Phys. Rev. Lett.* **88**, 257001 (2002).
65. Helm, T. et al. Correlation between Fermi surface transformations and superconductivity in the electron-doped high-T_c superconductor Nd2−xCexCuO4. *Phys. Rev. B* **92**, 094501 (2015).
66. Li, P., Balakirev, F. F. & Greene, R. L. High-field Hall resistivity and magnetoresistance of electron-doped $Pr_{2-x}Ce_xCuO_{4-\delta}$. *Phys. Rev. Lett.* **99**, 047003 (2007).
67. Sebastian, S. E. et al. Spin-order driven Fermi surface reconstruction revealed by quantum oscillations in an underdoped high T_c superconductor. *Phys. Rev. Lett.* **103**, 256405 (2009).
68. Altarawneh, M. M. et al. Superconducting pairs with extreme uniaxial anisotropy in URu_2Si_2. *Phys. Rev. Lett.* **108**, 066407 (2012).
69. Bastien, G. et al. Fermi-surface selective determination of the *g*-factor anisotropy in URu_2Si_2. *Phys. Rev. B* **99**, 165138 (2019).
70. Hundley, M. F., Thompson, J. D., Cheong, S-W., Fisk, Z. & Oseroff, S. B. Specific heat and anisotropic magnetic susceptibility of Pr_2CuO_4, Nd_2CuO_4 and Sm_2CuO_4 crystals. *Phys. C* **158**, 102–108 (1989).
71. Dalichaouch, Y., de Andrade, M. C. & Maple, M. B. Synthesis, transport, and magnetic properties of $Ln_{2-x}Ce_xCu0_{4-y}$ single crystals (Ln = Nd, Pr, Sm). *Physica C* **218**, 309–315 (1993).
72. Harrison, N., Hall, D. W., Goodrich, R. G., Vuillemin, J. J. & Fisk, Z. Quantum interference in the spin-polarized heavy Fermion compound CeB_6: evidence for topological deformation of the Fermi surface in strong magnetic fields. *Phys. Rev. Lett.* **81**, 870 (1998).
73. McCollam, A. et al. Spin-dependent masses and field-induced quantum critical points. *Phys. B* **359–361**, 1–8 (2005).

ACKNOWLEDGEMENTS

It is our pleasure to thank G. Knebel, H. Sakai, I. Sheikin, and A. Yaresko for illuminating discussions. This work was supported by HLD at HZDR, a member of the European Magnetic Field Laboratory (EMFL). P.D.G. acknowledges State Assignment #0033-2019-0001 for financial support and the Laboratoire de Physique Théorique, Toulouse, for the hospitality during his visit. R.G. acknowledges financial support from the German Research Foundation (Deutsche Forschungsgemeinschaft, DFG) via Germany's Excellence Strategy (EXC-2111-390814868). J.W. acknowledges financial support from the DFG through the Würzburg-Dresden Cluster of Excellence on Complexity and Topology in Quantum Matter - *ct.qmat* (EXC 2147, project-id 390858490).

AUTHOR CONTRIBUTIONS

T.H., F.K., M.K., E.K., W.B., and M.V.K. performed the experiments and analyzed the data. R.R., P.D.G., and M.V.K. initiated the exploration and performed the theoretical analysis and interpretation of the experimental results. H.F. and A.E. provided high-quality single crystals. R.R., P.D.G., T.H., W.B., E.K., J.W., R.G., and M.V.K. contributed to the writing of the manuscript.

COMPETING INTERESTS

The authors declare no competing interests.

ADDITIONAL INFORMATION

Supplementary information The online version contains supplementary material available at https://doi.org/10.1038/s41535-021-00309-6.

Correspondence and requests for materials should be addressed to R.R., T.H. or M.V.K.

Reprints and permission information is available at http://www.nature.com/reprints

Publisher's note Springer Nature remains neutral with regard to jurisdictional claims in published maps and institutional affiliations.